Structural characterization and skin penetration studies on sugar microneedles: Experimental and finite element modelling analyses

Eriketi Z. Loizidou[a,b], David A. Barrow*[b], Mark J. Eaton[b], John McCrory[b], Sam L. Evans[b], Chris J. Allender**[a]

[a]Cardiff University, School of Pharmacy, CF10 3NB, United Kingdom

[b]Cardiff University, School of Engineering, CF24 3AA, United Kingdom

* Corresponding author. Address: Cardiff School of Engineering, Cardiff University, 1-5 The Parade, Cardiff CF24 3AA, Cardiff, UK; Tel. +44(0)2920875921; Email address: barrow@cardiff.ac.uk

** Corresponding author. Address: School of Pharmacy, Cardiff University, Redwood Building, King Edward VII Ave, Cardiff CF10 3NB, Cardiff, UK; Tel. +44(0)2920875824; Email address: allendercj@cf.ac.uk

Abstract

Dissolving microneedles are especially attractive for transdermal drug delivery as they are associated with improved patient compliance and safety. Furthermore, microneedles made of sugars offer the added benefit of biomolecule stabilisation making them ideal candidates for delivering biological agents such as proteins, peptides and nucleic acids. In this study, we performed experimental and finite element analyses to study the mechanical properties of sugar microneedles and evaluate the effect of sugar composition on microneedle ability to penetrate the skin. Our results showed that microneedles made of carboxymethylcellulose/maltose and carboxymethylcellulose/trehalose are superior to those made of carboxymethylcellulose/sucrose in terms of both mechanical strength and skin penetration properties. Buckling was predicted to be the main mode of microneedle failure and the order of buckling was positively correlated to the Young's modulus values of the sugar constituents of each microneedle.

Keywords

Sugar microneedles, skin penetration, confocal microscopy, structural mechanics simulations, Young's modulus, buckling, von Mises stress

1. Introduction

Microneedles offer a promising approach for delivering therapeutic compounds through the skin, thus avoiding the gastrointestinal and hepatic first pass metabolism that can degrade the bioactive compounds, as well as the discomfort and pain associated with hypodermic delivery [1]. Furthermore, readily dissolving microneedles offer the added benefit of being able to either deliver secondary controlled delivery vectors or simple bolus dose.

Sugars are particularly attractive materials for delivering biomolecules via microneedles because in addition to, in the right combinations, forming mechanically strong microneedles that can penetrate the skin and rapidly dissolve, they are also known to act as stabilising agents. Sugars have commonly been used to increase the stability of nucleic acids and proteins, specifically saccharide excipients have been used to stabilise plasmid DNA [2] and human erythropoietin alfa [3] coated on the surface of microneedles. Additionally, sugars have been used in vaccine coating formulations for microneedle-mediated delivery [4–11]. Solid microneedle arrays made entirely out of sugars and encapsulating live recombinant human adenovirus type 5 have been shown to retain bioactivity, inducing potent multifunctional CD8+ T-cell responses, when administered through the skin of mice, at levels equivalent with conventional injectable routes [12]. In another example, human growth hormone (hGH) encapsulated within dissolving microneedle patches made of carboxymethylcellulose and trehalose demonstrated similar pharmacokinetics to conventional subcutaneous injections and retained activity for up to 15 months of storage at room temperature and humidity [13].

The forces that microneedles experience, when penetrating the skin, are typically dependent on microneedle material and geometry. The effect of microneedle geometry such as needle length, and shape (conical and pyramidal triangular and square) has been examined through experiments and computational modeling [14–17]. Studies using the numerical simulator ANSYS showed that circular microneedles experience less bending stress than rectangular and square pyramidal microneedles [14]. In a separate study square pyramidal microneedles demonstrated enhanced skin penetration compared to conical microneedles whilst simulation analysis also predicted a lower force of failure. The effect of material was also examined using the carbohydrates carboxymethyl cellulose and amylopectin as reference materials. Amylopectin, due to its higher Young's modulus value, proved to be a mechanically superior material for microneedles, compared to carboxymethyl cellulose [15].

In this study we performed a structural analysis of microneedles made from various sugar materials using both experimental measurements and modelling. Through systematic analysis we examined the effect of sugar composition on the mechanical properties of microneedles and their ability to penetrate the skin. Microneedle arrays of conical geometry, comprising of 1) carboxymethyl cellulose and sucrose (CMC/SUC), 2) carboxymethyl cellulose and maltose (CMC/MAL) and 3) carboxymethyl cellulose and trehalose dihydrate (CMC/TRD) at a 1:1 combination were prepared by the vacuum deposition method[18] and characterised by brightfield microscopy and SEM. Microneedle skin insertion was tested on porcine skin using brightfield / epi-fluoresence microscopy to study skin puncture and confocal microscopy to

study the skin penetration depth. Tensile tests were used to measure the Young's modulus values of the sugar compositions and finite element analysis, using the Structural Mechanics module of COMSOL Multiphysics was performed to evaluate the effects of material on the stresses experienced by the microneedles.

2. Material and methods

2.1 Microneedle fabrication

Microneedle arrays consisting of sodium carboxymethylcellulose (CMC) (average MW 250,000, Sigma-Aldrich, UK) and either sucrose, (SUC) (Sigma-Aldrich, UK), maltose, (MAL) (Sigma-Aldrich, UK) or trehalose dihydrate (TRD) (Sigma-Aldrich, UK) were prepared by the vacuum deposition method described by Martin *et al*.[18] Briefly, 200μl of 2% w/v solutions of sugar mixtures (1:1 w/w ratio of i) CMC/SUC, ii) CMC/MAL and iii) CMC/TRD) in water were injected onto a 1 cm^2 inverted cone shaped silicone micromould comprising 324 needles of 750 μm height, 200 μm base diameter, and 600 μm center-to-center spacing under vacuum. Following application of the sugar solutions, vacuum was released and the filled micromoulds were placed in a fume cupboard and allowed to dehydrate at room temperature for 3 days. The resulting microneedle arrays consisting of 1) 50 % CMC and 50 % SUC, 2) 50 % CMC and 50 % MAL and 3) 50 % CMC and 50 % TRD, were characterised by brightfield / epi-fluoresence microscopy (Nikon measuring microscope MM-800) and scanning electron microscopy (Carl Zeiss XB1540).

2.2 Skin penetration

The skin puncturing properties of the microneedles were studied on full-thickness cadaver porcine skin from which subcutaneous fat had been

removed. The skin was kept in the freezer until testing when it was thawed by briefly soaking in 37 ^{o}C water and then blow-dried. The sugar microneedles arrays (CMC / SUC, CMC / MAL and CMC / TRD) were applied to the skin for 30 seconds with gentle thumb pressure (~ 5N) that was applied for the duration of the test. The punctured skin surface was exposed to green tissue-marking dye (Fisher Scientific, UK) for 15 minutes after which any residual dye was wiped from the skin surface with tissue paper and swabbed clean with tap water. The treated skin was imaged and recorded under a microscope (Nikon measuring microscope MM-800). Confocal microscopy was used to determine the depth of skin penetration for each sugar microneedle array. Fluorescent sugar microneedles containing AlexaFluor 488 C5 maleimide, 50μg/ml, (Life Technologies Ltd, UK), were prepared in a procedure similar to the one described in Section 2.1 and skin penetration evaluated using full-thickness cadaver porcine skin previously incubated overnight in phosphate buffered saline (pH 7.4) containing 10 μg/ml Hoechst trihydrochloride trihydrate (Life Technologies Ltd, UK). The fluorescently labelled sugar microneedle arrays were applied to the skin with gentle thumb pressure and after 10 min were removed and the skin samples examined using a Leica SP5 confocal laser-scanning microscope equipped with an Ar laser and 20x objective.

2.3 Tensile tests

Digital Image Correlation (DIC) was used to measure the strain distributions during tensile evaluation. Displacement measurements were made using a Dantec Dynamics DIC system (Dantec Dynamics A/S, , Tonsbakken, Denmark) with two cameras and ISTRA4D software, on the

narrow part of a “dog bone” structure consisting of the sugar composites used to prepare the microneedles. The strain values used in the analysis were the average strains over the narrow part of the structures, as calculated by the DIC software. The “dog bone” structures of the three sugar materials (CMC / SUC, CMC / MAL and CMC / TRD) were prepared by first dissolving the sugar mixtures in water at 2 % w/v composition, and then layering the solutions on a PDMS sheet, which was left in a fume hood to dehydrate for 3 days. The resulting sugar film was cut to a “dog bone” shape using a template with a parallel gauge length 40mm long and 6.5mm wide.

2.4 Simulations

Simulations were performed using the Structural Mechanics Module of COMSOL Multiphysics (www.comsol.com). Simulations were performed on a single microneedle, the design of which was based on a 3D cone-shaped structure of dimensions 750 μm height, 200 μm base diameter and 10 μm tip diameter. The needle structures were treated as linear elastic materials using the Young’s modulus values and densities measured for each sugar composition (Table 1), and an estimated value of 0.3 for Poisson’s ratio. Two cylindrical structures were used to simulate the epidermis (including both the stratum corneum and viable epidermis) and dermis of the skin having the following dimensions, 600 μm diameter and 100 μm height for the epidermis and 600 μm diameter and 1000 μm height for the dermis. The skin structure was treated as a linear elastic material using 1 MPa as the Young’s modulus value for the epidermis [19] and 0.066 Mpa for the dermis[20]. Both epidermis and dermis were treated as nearly incompressible materials with Poisson’s ratio 0.495. The Solid Mechanics interface was used to define the quantities

and features for stress analysis, solving for the displacements. Von Mises stress and microneedle / skin deformation was simulated at static equilibrium using stationary analysis, during axial loading at the base of the needle for force values ranging from 0.1 to 17N. A fixed constrain was applied at the bottom surface of the dermis and movement of the needle base was allowed only for the axial direction. Linear buckling analysis was used to estimate the critical load at which the microneedle will become unstable. The critical load factor, of the microneedles was simulated during axial loading for 5N applied force, for the case where one end, the microneedle tip, is fixed in position and the other end, the microneedle base, is allowed to move only in the axial direction.

3. Results

3.1 Microneedle fabrication and characterisation

Sugar microneedles have been fabricated using different approaches including casting a viscous aqueous solution of sugars onto a microneedle inverse mould and then using centrifugation to force the liquid in to the mould [9,15] or by casting sugar-melts in the form of a microneedle array [21]. Microneedles made of maltose have also been prepared by stepwise controlled drawing lithography by controlling the drawing time and the solution viscosity [22]. In this study, we used vacuum deposition [18] to prepare the sugar microneedles. The methodology involves depositing a solution onto an inverse microneedle mould, so as to achieve complete coverage that is contained within an evacuated chamber. When the vacuum is released gas pressure forces the solution into the mould so as to completely fill the mould's micron-scale cavities. Using this approach microneedle arrays, were prepared

using three CMC / sugar composites (CMC / SUC, or CMC / MAL, or CMC / TRD). The resulting microneedle arrays were imaged by SEM and light-microscopy (Fig. 1) and were shown to possess close reciprocal geometries to the mould (750μm length, 200μm base diameter, 10μm tip diameter) and a tip-to-tip needle spacing of 600μm. The microneedle arrays were stored at ambient temperature and relative humidity and, based on microscopic observation, were capable of retaining an unchanged geometry for at least two months.

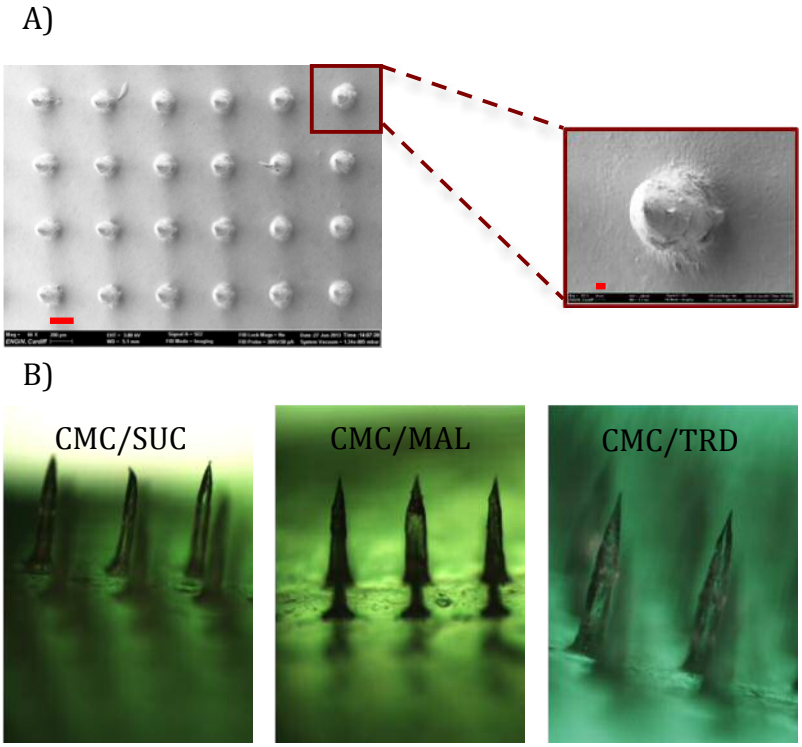

Figure 1: Sugar microneedle array images. A) Scanning electron micrographs of a CMC/TRD microneedle array at low magnification (scale bar = 200μm) and high magnification (scale bar = 20μm). B) Microscopic images with x5 magnification of a CMC/SUC, CMC/MAL and CMC/TRD array.

3.2 Skin penetration studies

Skin penetration was tested in *ex vivo* porcine skin samples with the aim of assessing both ability and depth of microneedles penetration. Disruption of stratum corneum was evident for all skin samples and the

breach locations were observed with separation distances of approximately 550μm, consistent with the microneedle array spacing (Fig. 2B). Furthermore, microscopic observation of the microneedles after skin puncture showed that the microneedles remained intact. Evidence of bending at microneedle tips was clear throughout the array for the CMC/SUC arrays while for the CMC/MAL and CMC/TRD arrays tip-bending was observed only for microneedles located at the edge of the arrays.

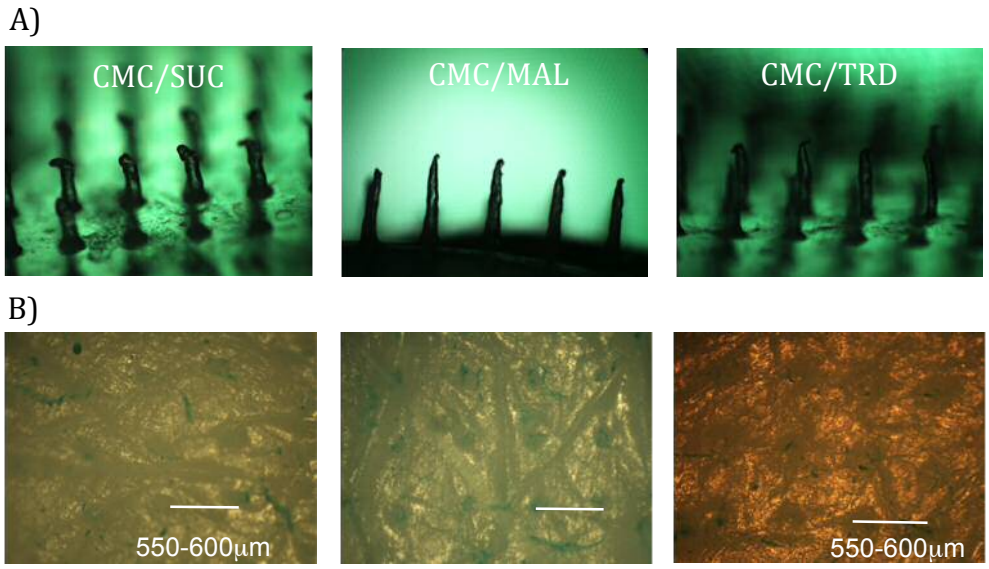

Figure 2: A) Microscopic images of microneedle arrays of CMC/SUC, CMC/MAL, CMC/TRD, after being inserted into the skin for 30s B) Microscopic images of the punctured skin after testing with CMC/SUC, CMC/MAL, CMC/TRD microneedles, for 30s.

Confocal microscopy was subsequently used to evaluate the depth of skin penetration using fluorescently labelled microneedles. Maximum fluorescence depth at 5 skin breach locations, per sample, was measured and a mean value determined (Fig. 3). Maximum mean fluorescence depths of 35 μm for CMC / SUC microneedles, 90 μm for CMC / MAL microneedles and 65 μm for the CMC / TRD microneedles were recoded. The actual depth of skin penetration is likely to be deeper than those measured in this confocal

experiment since the technique has limited detection sensitivity, due to significant attenuation and scatter of both excitation and emission wavelengths by the epidermis [23].

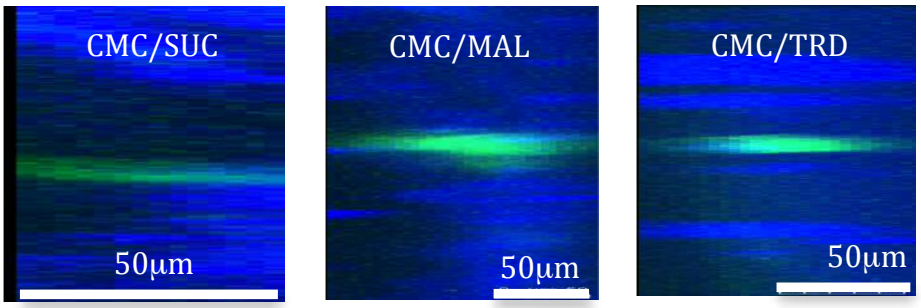

Figure 3: Z-stack images of punctured skin after being tested with fluorescently-labelled microneedles of CMC/SUC, CMC/MAL, and CMC/TRD sugar compositions, for 10min. Green colour represents the recorded fluorescence due to the diffusion of AlexaFluor488 from the microneedles to the skin (top of the skin is at the left-hand side).

3.3 Structural analysis

The mechanical properties of the sugar materials were initially assessed using the load acquired from the test machine and the strain measurements calculated by the DIC analysis. Knowledge of the specimen dimensions allowed the stress to be calculated from the load and so plots of stress against strain were generated (Fig. 4). The CMC / MAL and CMC / TRD sugar combinations showed linear behavior up to the point of failure by fracture that is typical of brittle materials, such as glass. On the other hand, the CMC / SUC sugar combination gave a more flexible material with slight evidence of non-linearity at small strains. However, the linearly elastic region was prominent and a Young's modulus value was derived. In addition, ultimate tensile strengths were determined at the highest point in the stress / strain curves. The values (Table 1) were subsequently used in microneedle structural mechanics simulations.

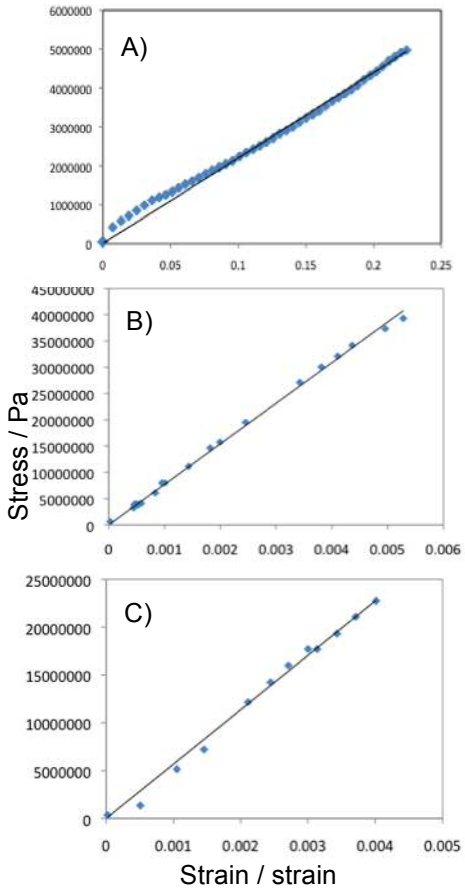

Figure 4: Stress vs. strain curves obtained from tensile tests for the sugar materials consisting of 1:1 ratio of A) CMC/SUC, B) CMC/MAL and C) CMC/TRD.

Table 1. Young's modulus and ultimate tensile strength for CMC / SUC, CMC / MAL, and CMC / TRD sugar compositions.

Sugar composition at a 1:1 ratio	**Density**	**Young's modulus**	**Ultimate tensile strength**
CMC/SUC	1624 Kg/m^2	2.20e7 Pa	2.21e7 Pa
CMC/MAL	1812 Kg/m^2	7.42e9 Pa	7.44e9 Pa
CMC/TRD	1439 Kg/m^2	5.69e9 Pa	5.66e9 Pa

Computationally, the compressive forces acting on the microneedle can be described by the calculated von Mises stress, which refers to the combined principal stresses (in the x, y, z dimensions) acting on an elastic body that is subject to a system of loads. The von Mises values can be used to predict whether a particular design will fail; this will occur if the maximum value of the von Mises stress induced in the material is more than the fracture

strength of the material. Furthermore, slender structures often show sudden failure when subject to compressive loads even though the stress at the point of failure is less than the maximum stress that the material can withstand. This mode of failure is known as buckling and can be studied computationally using a linear buckling analysis to estimate the critical load factors. In our simulation analysis we considered an ideal situation where a coaxial force is applied at the base of the microneedle giving rise to compressive and buckling forces only, treating bending forces as negligible. Stationary and linear buckling analyses were employed to solve for the von Mises stresses and the critical buckling loads in a single microneedle with conical geometry and dimensions matching the tested microneedles. Although the skin is not linearly elastic [24] and its deformation may not have been accurately predicted, the microneedle material did exhibit linear behaviour and therefore, a linear elastic model was deemed appropriate to predict the load/stress for the needles. Figure 5A shows a 3D plot of the surface von Mises stress calculated when an axial load is applied to the base of the microneedle. The areas coloured in red depict the areas that experience the most stress.

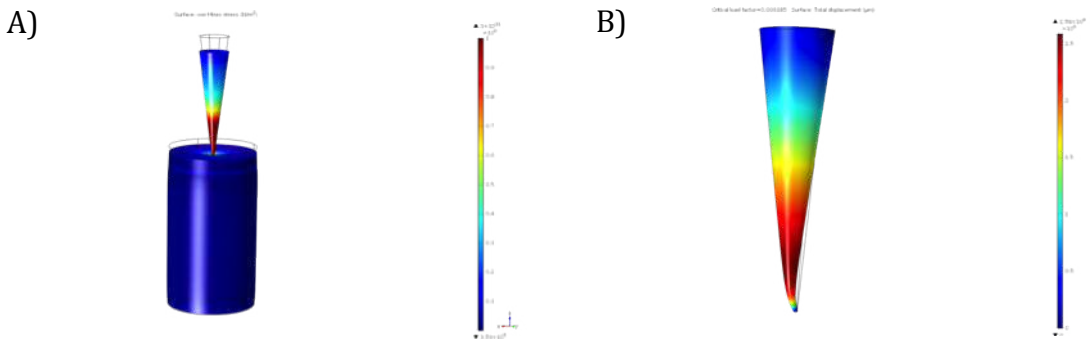

Figure 5: A) Finite element analysis of the surface von Mises stress when axial load, 5N, is applied on the base of a CMC/MAL microneedle of conical shape. The skin is simulated as a union of cylindrical structures comprising the epidermis and dermis. B) Buckling mode prediction for a CMC/MAL microneedle when axial load is applied at the base of the microneedle and a fixed constraint is forced at the tip of the microneedle.

The predicted stresses were calculated for a single needle and adapted for a 18 x 18 microneedle array by dividing by the total number of the needles in the array (Table 2). A parametric sweep of applied forces was used until the predicted stress values for the microneedle arrays reached the values of the ultimate tensile strength for their corresponding sugar material. The calculated von Mises stresses for the CMC/SUC microneedles exceed the ultimate stress value for the material constituent, 2.21e7 Pa, when the applied force exceeds 0.1N. On the other hand, the von Mises stresses for the more rigid CMC / MAL and CMC / TRD sugar constituents, do not reach their ultimate tensile stress values until the applied forces exceed 17N and 13N, respectively.

Table 2. Calculated von Mises stresses for a CMC / SUC, CMC / MAL and CMC / TRD microneedle. Values were measured using the Structural Mechanics module of COMSOL Multiphysics for a single microneedle based on which a value was estimated for an 18 x 18 array. The values highlighted in bold indicate the approximate force at which the predicted von Mises stresses reach the ultimate tensile strength of the material.

F (N)	**SUC – von Mises (Pa)**		**MAL-von Mises (Pa)**		**TRD-von Mises (Pa)**	
	Per needle	18x18 array	Per needle	18x18 array	Per needle	18x18 array
0.1	7.40e9	**2.28e7**	1.43e10	4.41e7	1.43e10	4.41e7
1	7.40e10	2.28e8	1.43e11	4.41e8	1.43e11	4.41e8
2	1.48e10	4.57e8	2.86e11	8.83e8	2.86e11	8.83e8
3	2.21e11	6.58e8	4.29e11	1.32e9	4.29e11	1.32e9
4	2.96e11	9.13e8	5.72e11	1.76e9	5.72e11	1.76e9
5	3.70e11	1.14e9	7.17e11	2.21e9	7.15e11	2.21e9
10	7.40e11	2.28e9	1.43e12	4.41e9	1.43e12	4.41e9
13	9.63e11	2.97e9	1.86e12	5.47e9	1.86e12	**5.74e9**
15	1.11e12	3.43e9	2.15e12	6.63e9	1.43e12	4.41e9
17	1.26e12	3.89e9	2.43e12	**7.50e9**	2.43e12	7.50e9

Linear buckling analysis was performed to evaluate the force of failure due to buckling for the three sugar microneedle arrays. The predicted critical load factor, λ, for the microneedle was predicted for an applied force of 5N

and the critical buckling force was obtained by multiplying the applied force by the critical load factor. When the applied force is higher than the critical buckling force, or when the critical load factor, λ, has values less than 1, then buckling occurs. The predicted critical load factors for the single microneedles were adapted for an 18 x 18 microneedle array by multiplying by the total number of the needles in the array (Table 3).

Table 3. Calculated critical load factors, λ, and critical loads, $F_{crit.}$, for a CMC / SUC, CMC / MAL and CMC / TRD microneedle. Values were measured using the Structural Mechanics module of COMSOL Multiphysics for a single microneedle based on which a value was estimated for an 18 x 18 array. The applied force used for the buckling analysis was 5N.

Sugar	**λ**		**$F_{crit.}$ (N)**
	Per needle	18x18 array	18x18 array
CMC/SUC	2.72e-5	0.0088	0.04
CMC/MAL	0.0092	3.0	15
CMC/TRD	0.0070	2.3	11

The critical buckling force for the array is estimated by multiplying the predicted critical load factors by the applied load. Based on these results, the critical buckling force for the sugar microneedle arrays was calculated to be 0.04 N for CMC / SUC, 15 N for CMC / MAL and 11 N for CMC / TRD. This indicates that microneedle arrays made of CMC / SUC are likely to experience failure due to buckling as the required force of insertion to the skin [25] is higher than their critical buckling force. On the other hand, the values of the critical buckling forces for the CMC / MAL and CMC / TRD microneedles are much higher than the insertion forces indicating that both arrays can be inserted in the skin without failing from buckling. Figure 5B shows the predicted buckling mode and the point-of-failure, which is the area coloured in red. The same buckling mode has been predicted for all the sugar microneedles.

4. Discussion

Sugar microneedles are particularly attractive vesicles for delivering biological agents because they both facilitate safe and rapid delivery through the skin and offer improved biomolecule stability. While sugar based microneedles are useful materials for incorporating biomacromolecules, the resultant device can have storage and stability problems itself due to their inherent hygroscopic nature leading to instability and poor storage prognosis at ambient relative humidities [26]. One way of increasing the long-term stability of sugar microneedles is by combining different substituents of different elasticity and rigidity. Celluloses are known to be stiffer materials than sugars [27] and mechanically strong microneedles have been made by combining carboxymethylcellulose and lactose [12].

Most published studies on sugar microneedles focus on the delivery potential of devices and not on structural aspects of the microneedles themselves. Systematic mechanical analysis of microneedles, is highly desirable since this would provide insight into their practical usefulness as drug delivery systems and whether they will be effective in a given application. In this work we prepared sugar microneedles by combining the disaccharides, sucrose, maltose or trehalose, with the polysaccharide, carboxymethylcellulose. The aim was to produce mechanically strong, yet rapidly dissolving, microneedles by manipulating the elastic properties of sugar combinations and to investigate the effect that the choice of material has on the mechanical and skin penetration properties of the microneedles.

When microneedles are applied to the surface of the skin they will easily be deformed due to its viscoelastic properties. As such, the design and

choice of material will have a critical role in determining whether they will effectively penetrate the skin. Assuming that a microneedle is loaded into the skin with coaxial force, then the typical forces that the microneedle will experience are compressive and buckling. In real applications however, lateral movements are also generated giving rise to bending forces as well. In an ideal situation the bending forces can be ignored so that the compressive and buckling become the main forces acting on the microneedles. For slender, high aspect ratio microneedle geometries, buckling is most likely to be the major mode of mechanical failure [16]. Accordingly in this study, buckling was observed, mainly for the sugar microneedles made of CMC/SUC whereas, none of the microneedles tested experienced failure from fracture.

The critical buckling load for a microneedle (F) can be described by Euler's buckling formula for a cylindrical column, (Eq. 1), where *E*, is the elasticity factor of a material described by Young's modulus, *d*, the area moment of inertia that is dependent on geometry, *K*, the column effective factor that is determined by the boundary conditions and *L* the unsupported length of the column.

$$F = \frac{E\pi^3 d^4}{64(KL)^2} \qquad Eq.1$$

All other factors being equal, as in this case for sugar microneedles possessing the same geometry, then based on Euler's formula the elasticity of the material will determine the critical buckling load. Consequently, based on the Young's modulus values for the three sugar constituents (Table 1), the critical load that CMC / SUC microneedles can withstand before buckling

would be much lower than that for CMC / TRD and CMC / MAL microneedles. Based on the simulations the CMC / SUC microneedles are likely to buckle when the applied axial force exceeds 0.04N. The typical force that is required for a microneedle array to puncture the skin can be as low as 0.1N [25], depending on microneedle material and geometry, and consequently, the CMC/SUC microneedles should fail from buckling before skin penetration is achieved. Interestingly, the predicted buckling mode for the microneedles shows the point of failure to be slightly above the tip (Fig. 5B). This indicates that even in the event when the insertion force is higher than the critical buckling threshold, as is the case of the CMC / SUC microneedles, the microneedles may still puncture the skin and penetrate to a certain depth before failing. The depth of skin penetration can be correlated to the critical buckling force. Best skin penetration was demonstrated by CMC / MAL microneedles. These also had the highest predicted critical buckling force (closely followed by the CMC / TRD microneedles). Finally, the CMC / SUC microneedles, that penetrated least effectively, had the lowest predicted critical buckling force. Combined these results suggest that whereas the CMC / SUC microneedles are unlikely to be of any practical use, microneedles made from CMC / MAL and CMC / TRD are likely to sufficiently penetrate the skin without failing.

Conclusions

Despite the great therapeutic potential presented by solid dissolving microneedles, useful demonstration of their efficacy has been limited, mainly due to weak mechanical strength. Methods for measuring the mechanical

properties and for predicting performance of dissolving microneedles are therefore highly desirable. In this study we undertook experimental and computational analyses to investigate the mechanical properties of sugar microneedles. Both predictions and experiments showed that microneedles made of CMC / MAL and CMC / TRD are superior to those made of CMC / SUC in terms of both mechanical strength and skin penetration properties. Simulation analyses revealed the main reason for mechanical failure to be buckling and showed a correlation between the Young's modulus of the sugar constituents and the predicted critical buckling load of the microneedles and the depth of skin penetration. The fact that an agreement between experimental data and simulation could be demonstrated, shows that computational models can be useful to provide a qualitative view as to how a microneedle device will behave when pushed on to the surface of the skin. This, therefore, appears to be a valuable approach for predicting microneedle performance, and therefore for guiding design and materials selection, prior to fabrication.

Acknowledgments

The assistance of Dr Emmanuel Brousseau with SEM and Dr Edward Sayers with confocal microscopy is gratefully acknowledged. This study was supported by the Marie Curie Industry-Academia Partnerships and Pathways FP7-PEOPLE-2009-IAPP-251630 grant, *HIPODERM*.

References

[1] Y.-C. Kim, J.-H. Park, M.R. Prausnitz, Microneedles for drug and vaccine delivery, Adv. Drug Deliv. Rev. 64 (2012) 1547–1568.

[2] M. Pearton, V. Saller, S.A. Coulman, C. Gateley, A.V. Anstey, V. Zarnitsyn, et al., Microneedle delivery of plasmid DNA to living human skin: Formulation coating, skin insertion and gene expression, J. Controlled Release. 160 (2012) 561–569.

[3] E.E. Peters, M. Ameri, X. Wang, Y.-F. Maa, P.E. Daddona, Erythropoietin-coated zp-microneedle transdermal system: Preclinical formulation, stability, and delivery, Pharm Res. 29 (2012) 1618–1626.

[4] Y.C. Kim, F.-S. Quan, R.W. Compans, S.-M. Kang, M.R. Prausnitz, Formulation of microneedles coated with influenza virus-like particle vaccine, AAPS PharmSciTech. 11 (2010) 1193–1201.

[5] C. Edens, M.L. Collins, J. Ayers, P.A. Rota, M.R. Prausnitz, Measles vaccination using a microneedle patch, Vaccine. 31 (2013) 3403–3409.

[6] W.C. Weldon, M.P. Martin, V.G. Zarnitsyn, B.Z. Wang, D.G. Koutsonanos, I. Skountzou, et al., Microneedle vaccination with stabilized recombinant influenza virus hemagglutinin induces improved protective immunity, Clin Vaccine Immunol. 18 (2011) 647–654.

[7] A. Vrdoljak, M.C. McGrath, J.B. Carey, S.J. Draper, A.V.S. Hill, C. O'Mahony, et al., Coated microneedle arrays for transcutaneous delivery of live virus vaccines, J. Controlled Release. 159 (2012) 34–42.

[8] F.E. Pearson, C.L. McNeilly, M.L. Crichton, C.A. Primiero, S.R. Yukiko, G.J. Fernando, et al., Dry-Coated Live Viral Vector Vaccines Delivered by Nanopatch Microprojections Retain Long-Term Thermostability and Induce Transgene-Specific T Cell Responses in Mice, PLoS One. 8 (2013) e67888.

[9] S. Kommareddy, B.C. Baudner, S.-J. Oh, S.-Y. Kwon, M. Singh, D.T. O'Hagan, Dissolvable microneedle patches for the delivery of cell-cultured-derived influenza vaccine antigens, J. Pharm. Sci. 101 (n.d.) 1021–1027.

[10] Y.-C. Kim, F.-S. Quan, R.W. Compans, S.-M. Kang, M.R. Prausnitz, Formulation and coating of microneedles with inactivated influenza virus to improve vaccine stability and immunogenicity, J. Controlled Release. 142 (2010) 187–195.

[11] Y.C. Kim, F.-S. Quan, J.M. Song, A. Vunnava, D.G. Yoo, K.M. Park, et al., Influenza immunization with trehalose-stabilized virus-like particle vaccine using microneedles, Proc Vaccinol. 2 (2010) 17–21.

[12] V. Bachy, C. Hervouet, P.D. Becker, L. Chorro, L.M. Carlin, S. Herath, et al., Langerin negative dendritic cells promote potent CD8+ T-cell priming by skin delivery of live adenovirus vaccine microneedle arrays, PNAS. 118 (2013) 8–13.

[13] J.W. Lee, S.O. Choi, E.I. Felner, M.R. Prausnitz, Dissolving microneedle patch for transdermal delivery of human growth hormone, Small. 7 (2011) 531–539.

[14] R. Aggarwal, C.R. Johnston, Geometrical effects in mechanical characterizing of microneedle for biomedical applications, Sens. Actuators B. 102 (2004) 226–234.

[15] J.W. Lee, J.-H. Park, M.R. Prausnitz, Dissolving microneedles for transdermal drug delivery, Biomaterials. (2008) 2113–2124.
[16] J.-H. Park, M.R. Prausnitz, Analysis of the Mechanical Failure of Polymer Microneedles by Axial Force, J. Korean Phys. Soc. 56 (2010) 1223–1227.
[17] R.F. Donnelly, M.J. Garland, D.I.J. Morrow, K. Migalska, T.R.R. Singh, R. Majithiya, et al., Optical coherence tomography is a valuable tool in the study of the effects of microneedle geometry on skin penetration characteristics and in-skin dissolution, J. Controlled Release. 147 (2010) 333–341. doi:10.1016/j.jconrel.2010.08.008.
[18] C.J. Martin, C.J. Allender, K.R. Brain, A. Morrissey, J.C. Birchall, Low temperature fabrication of biodegradable sugar glass microneedles for transdermal drug delivery applications, J. Controlled Release. 158 (2012) 93–101.
[19] M. Geerligs, L. van Breemen, G. Peters, P. Ackermans, F. Baaijens, C. Oomens, In vitro indentation to determine the mechanical properties of epidermis, J. Biomech. 44 (2011) 1176–1181.
[20] Y. Hara, Y. Masuda, T. Hirao, N. Yoshikawa, The relationship between the Young's modulus of the stratum corneum and age: a pilot study, Skin Res. Technol. Off. J. Int. Soc. Bioeng. Skin ISBS Int. Soc. Digit. Imaging Skin ISDIS Int. Soc. Skin Imaging ISSI. 19 (2013) 339–345. doi:10.1111/srt.12054.
[21] T. Miyano, Y. Tobinaga, T. Kanno, Y. Matsuzaki, H. Takeda, M. Wakui, et al., Sugar micro needles as transdermic drug delivery system, Biomed. Microdevices. 7 (2005) 185–188.
[22] K. Lee, C.Y. Lee, H. Jung, Dissolving microneedles for transdermal drug administration prepared by stepwise controlled drawing of maltose, Biomaterials. 32 (n.d.) 3134–3139.
[23] L.J. Mortensen, C.E. Glazowski, J.M. Zavislan, L.A. DeLouise, Near-IR fluorescence and reflectance confocal microscopy for imaging of quantum dots in mammalian skin, Biomed. Opt. Express. 2 (2011) 1610–1625. doi:10.1364/BOE.2.001610.
[24] R.B. Groves, S.A. Coulman, J.C. Birchall, S.L. Evans, Quantifying the mechanical properties of human skin to optimise future microneedle device design, Comput. Methods Biomech. Biomed. Engin. 15 (2012) 73–82.
[25] S.P. Davis, B.J. Landis, Z.H. Adams, M.G. Allen, M.R. Prausnitz, Inserion of microneedles into skin: measurement and prediction of insertion force and needle fracture force, J. Biomech. 37 (2004) 1155–1163.
[26] R.F. Donnelly, D.I.J. Morrow, T.R.R. Singh, K. Migalska, P.A. McCarron, C. O'Mahony, et al., Processing difficulties and instability of carbohydrate microneedle arrays, Drug Dev. Ind. Pharm. 35 (2009) 1242–1254. doi:10.1080/03639040902882280.
[27] F. Bassam, P. York, R.C. Rowe, R.J. Roberts, Young's modulus of powders used as pharmaceutical excipients, Int. J. Pharm. 64 (1990) 55–60.